Second harmonic generation in magnetic nanoparticles with vortex magnetic state

V. L. Krutyanskiy,[1] I. A. Kolmychek,[1] B. A. Gribkov,[2] E. A. Karashtin,[2] E. V. Skorohodov,[2] and T. V. Murzina[1]
[1]*Department of Physics, Moscow State University, 119991 Moscow, Russia*
[2]*Institute for Physics of Microstructures RAS, Nizhny Novgorod 603950, GSP-105, Russia*
(Received 8 July 2013; revised manuscript received 21 August 2013; published 19 September 2013)

Nonlinear optical properties of a regular array of triangular-shaped vortex magnetic nanoparticles is studied using the optical second harmonic generation (SHG) technique. We demonstrate that the SHG azimuthal anisotropy is consistent with the $3m$ symmetry of individual Co nanodots placed in a square surface lattice. Qualitatively different SHG magnetic hysteresis loops are obtained for circular and linear polarizations of the fundamental radiation. In the first case, a wide SHG hysteresis at zero DC magnetic field H is observed, which is attributed to a macroscopic magnetic toroid moment in Co nanodots induced by a noncentrosymmetric distribution of the magnetization. On the contrary, for the linear pump polarization the SHG loop is similar to observed commonly in linear magnetooptics for vortex magnetic structures and reveals a rather narrow width at $H = 0$. A phenomenological SHG description based on the introduction of the SHG polarization induced by a magnetic toroid moment in vortex magnetic nanostructures is presented.

DOI: 10.1103/PhysRevB.88.094424 PACS number(s): 78.67.Qa, 78.20.Ls, 78.67.Bf

I. INTRODUCTION

Optical second harmonic generation has demonstrated its unique possibilities to the studies of magnetic nanostructures. Various types of effects have been observed using this technique, including size effects,[1–3] geometrical resonances,[4–6] plasmon excitation,[7,8] etc. Composition of nanomaterials with unique properties is of high interest, as they can bring about very special physical and technological realizations. Much attention is attracted to magnetic nanostructures, first of all due to a possibility of making magnetic memory devices based on such systems.[9] It was demonstrated[10] that depending on their composition and geometry, nanostructures can reveal magnetic toroid moment, similarly to ferrotoroid domains observed in Ref. 11. Besides, chirality of vortex magnetic nanoelements can be switched by an external magnetic field.[12] On the contrary to the uniform magnetization, magnetic toroid moment intrinsically exists in magnetic structures with spatially noncentrosymmetric distribution of the magnetization. It is an additional mechanism that results in the breaking down of the time reversal symmetry in such structures and hence should lead to the appearance of new interesting optical effects.

Vortex magnetization was studied mostly in individual nanodots using magnetic force microscopy and magnetic transmission soft x-ray microscopy,[13] while the task remained to achieve a uniform vorticity within an ensemble of magnetic nanoparticles. This problem was solved by the composition of regular arrays of magnetic nanodots of noncentrosymmetric shape.[14,15] Here the idea of an asymmetry of nanodots' structure for the formation of magnetic vortices was exploited. The symmetry with respect to spatial inversion and time reversal operations is broken in such structures due to a nonuniform magnetic moment distribution. That leads to the existence of nonreciprocal optical effects first observed in Ref. 14. Optical second harmonic generation (SHG) is known for its intrinsically high sensitivity to the main properties of nanostructures, including magnetic and magnetoplasmonic ones.[16–20] The SHG was shown to be a promising tool for studying structures with antiferromagnetic or ferrotoroidal ordering.[21,22] A violation of spatial inversion symmetry is also necessary for the SHG process.

In this paper the SHG probe is applied to visualize the vortex magnetization state of regular arrays of triangular-shaped cobalt nanoparticles. The main point here is that due to a chosen design of the samples, a macroscopic magnetic vortex state can be formed by application of an external DC magnetic field. We demonstrate that the vortex magnetic state modifies the SHG hysteresis loops and thus allows us to distinguish the vortex magnetic state of a regular array of magnetic nanodots. A phenomenological description of the SHG process in such structures is discussed.

II. SAMPLES AND EXPERIMENTAL SETUP

The structure under study is a 2D square lattice of triangular-shaped cobalt dots made by the electron beam lithography and lift-off technique on the surface of an amorphous silica plate. The deposition procedure is described in detail in Ref. 23. The thickness of the magnetic structures is 30 nm, a typical size of the Co triangle's side is 0.7 μm, and the period of the lattice is 1.4 μm.

The composed nanostructures reveal a vortex magnetization state in the absence of the external magnetic field. A noncentrosymmetric shape of a single element along with the regular distribution of nanoparticles on the substrate, result in the macroscopic vortex magnetization after the external DC magnetic field is applied along the sides of the triangular particles. The corresponding magnetic state visualized by MFM technique is shown in Fig. 1. On the contrary, after the structure was magnetized along the height of the triangles, the particles with clockwise and counterclockwise vortices are formed, so that the average vortex magnetization is zero. Thus the appearance of vorticity in the optical response of such structures can be studied when using different magnetization geometry.

SHG experiments were performed using the linearly or circularly polarized radiation of a Ti:Sapphire laser operating at the wavelength of 780 nm, with the pulse duration of 100 fs

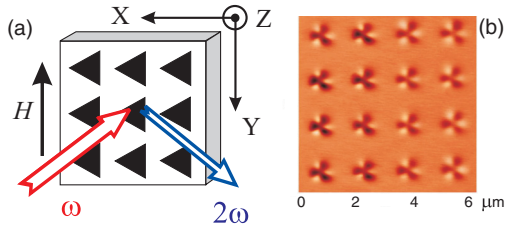

FIG. 1. (Color online) (a) Scheme of the light interaction with the sample; (b) MFM image of a homogeneous vortex magnetic state of the sample.

and the average power of 100 mW. The pump radiation was focused on the surface of the sample into a spot of 50 μm in diameter, the angle of incidence being 40°. Second harmonic radiation at 390 nm reflected from the sample passed through an analyzer and necessary set of colored filters and was detected by a PMT. The anisotropy of the SHG response was studied when the sample was rotated around its normal, the polarization of the fundamental and second harmonic radiation being fixed.

Magnetization-induced effects in SHG were studied in the transversal geometry, as the magnetic field was applied in the plane of the sample, along the side or the height of the Co triangles. Computer controlled electromagnet was used to change the magnetic field so that the magnetic hysteresis loops in the SHG intensity could be measured.

III. EXPERIMENTAL RESULTS

A. SHG anisotropy measurements

Prior to the magnetic measurements, the azimuthal SHG anisotropy was studied in transmission through the sample at normal incidence. The measurements were performed for the demagnetized sample, i.e., after the removal of the magnetic field applied along the height of the triangles. In other words both average vortex moment and magnetization were zero and the SHG anisotropy revealed purely the symmetry of a nonmagnetic SHG response.

Figure 2(a) shows the SHG anisotropic patterns as the linearly polarized fundamental radiation was used, its polarization plane being parallel or perpendicular with respect to the second harmonic polarization. A clear sixfold symmetry of the SHG patterns can be seen, that is consistent with the 3*m* symmetry of triangular-shaped particles. Zero azimuthal angle corresponds to the case as linear fundamental polarization is parallel to the sides of the triangular particles.

Azimuthal dependencies for the parallel and crossed polarizations of the fundamental and SHG radiation shown in Fig. 2(a) are shifted on the angular scale. This proves that the observed azimuthal dependencies are attributed to anisotropy of the studied structure. An isotropic background is probably the result of the Hyper-Rayleigh scattering at the SHG wavelength in our spatially inhomogeneous structure.[24]

Figure 2(b) presents the SHG anisotropic patterns measured for the left- or right-circularly polarized fundamental radiation. A clear threefold symmetry of the SHG pattern exists, which proves again that the SHG symmetry is governed by the symmetry of the second-order nonlinear-optical response of

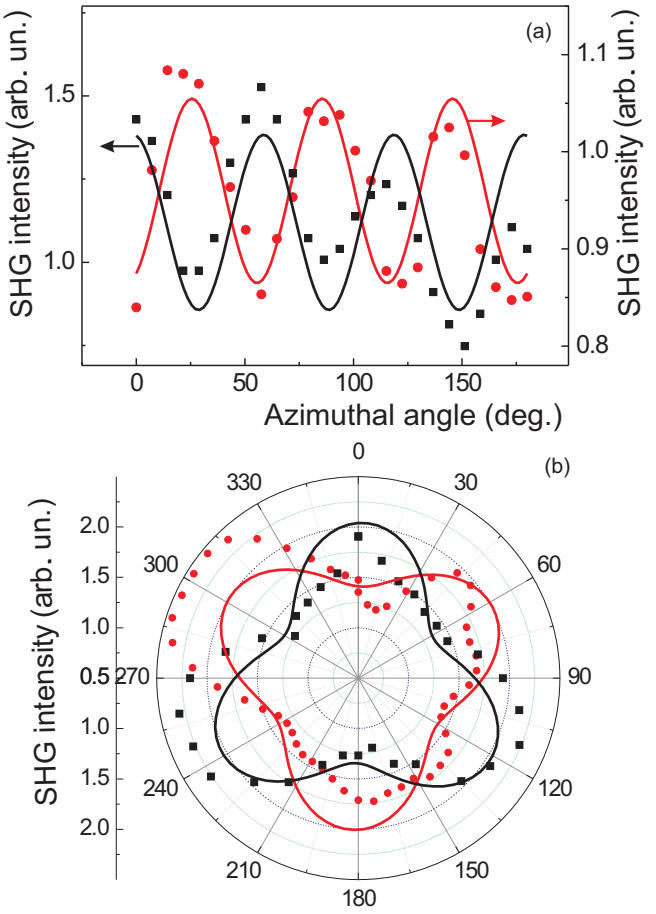

FIG. 2. (Color online) Azimuthal anisotropy patterns of linearly polarized SHG measured for the normal incidence of the fundamental radiation with (a) linear polarization that is parallel (black squares) or perpendicular (circles) with respect to fundamental beam polarization, and (b) left (black squares) or right (circles) circularly polarized fundamental radiation. Azimuthal orientation of the samples corresponds to the case as the sides of the Co triangles are parallel to the plane of incidence of the fundamental beam. Lines are the result of the approximation.

an individual magnetic particle. This conclusion is reasonable if we take into account that the size of a particle is comparable with the wavelength of the fundamental light, thus the effects of the particles shape along with the retardation effects within it form the coherent SHG response of the whole ensemble.

B. Magnetic-field induced SHG effects

1. Linearly polarized fundamental radiation

Magnetization-induced nonlinear optical effects were studied in the geometry of the transversal magneto-optical Kerr effect for specularly reflected SHG. In order to reveal the vortex magnetization state, the SHG measurements were performed for the two cases, as the sample was magnetized along the side of the triangles (which leads to a macroscopic vortex magnetization of an array of nanodots) and along their height (so that the vortices are randomly oriented in the structure).

The SHG hysteresis loop for the magnetization along the triangles' side shown in Fig. 3 were measured for the

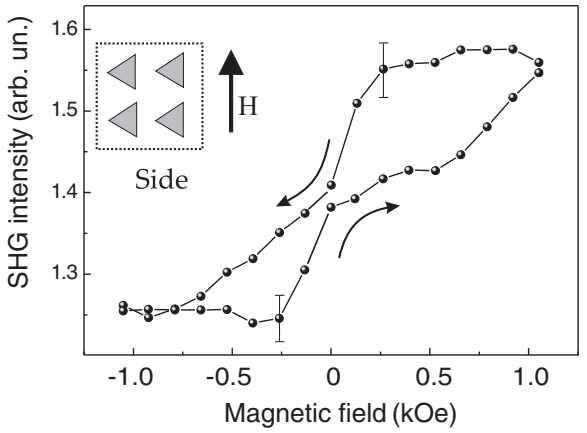

FIG. 3. SHG hysteresis loop measured under the excitation of the magnetic structure by p-polarized fundamental radiation and for the DC magnetic field that is parallel to the side of Co triangles.

p-polarized fundamental and SHG waves. This corresponds to the macroscopic vortex magnetization, which is maximal for $H = 0$. The shape of the SHG hysteresis loop is similar to commonly observed for vortex magnetic structures and reveals a very small width at zero magnetic field. Similar SHG dependence was observed after the Co triangles were magnetized along their height so that a random vortex magnetization was formed.

At the same time, a strong modulation of the SHG intensity induced by the homogeneous magnetic field can be seen in both cases. It can be characterized by the SHG magnetic contrast, that is commonly introduced as $\rho_{2\omega} = \frac{I_{2\omega}(+)-I_{2\omega}(-)}{I_{2\omega}(+)+I_{2\omega}(-)}$, where $I_{2\omega}(+)$ and $I_{2\omega}(-)$ are the SHG intensities for the opposite directions of the external magnetic field.[17] In the considered structures and for the saturating magnetic fields of ± 1.2 kOe we obtain $\rho_{2\omega} \approx 10\%$, that is a typical value for ferromagnetic metals.

2. *Circularly polarized fundamental radiation*

While vortex magnetization of nanoparticles is not much pronounced for the linear polarizations of the pump radiation, our experiments show that the opposite vortex magnetic states can be clearly distinguished when using the circularly polarized pump beam. Figures 4(a) and 4(b) show the dependencies of the p-polarized SHG intensity on the external magnetic field for that case. It can be seen that the shape of the SHG hysteresis loops differs from that obtained for the linearly polarized fundamental radiation (see Fig. 3 for comparison). The most clear difference is that the SHG hysteresis loop at $H = 0$ is rather wide for the circular fundamental radiation. The quantity that can lead to this difference is the macroscopic toroid moment $\mathbf{T}$ that is induced by average vortex magnetization of nanoparticles and will be discussed in the next section. Here it is worth noting that $\mathbf{T}$ reaches its maximal value for the zero magnetic field.

To check whether this difference in the SHG hysteresis loops is due to the nonzero macroscopic magnetic vorticity, a similar experiment was performed for magnetization along the triangles' height, i.e., for the zero macroscopic vortex magnetization. The corresponding experimental SHG dependence

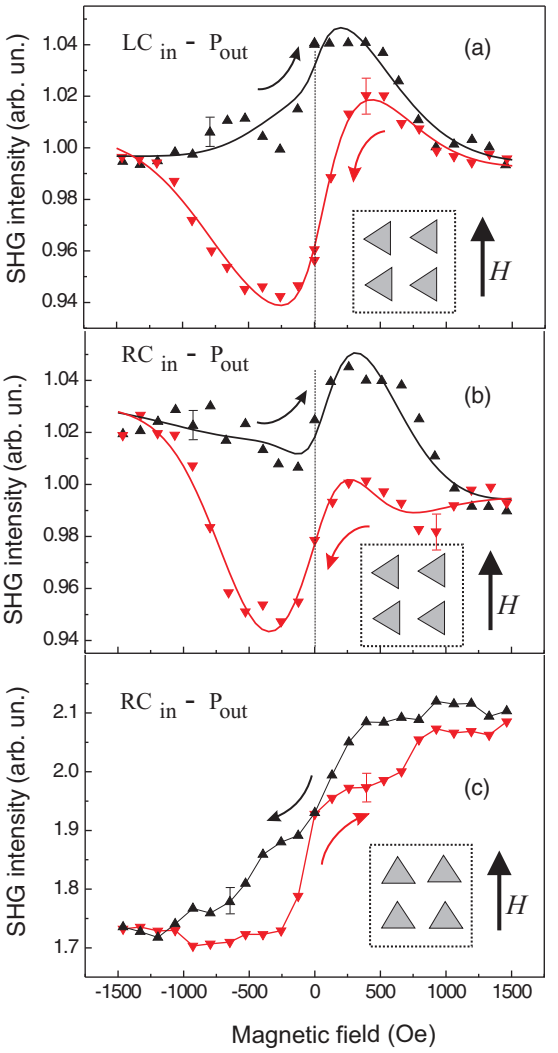

FIG. 4. (Color online) Hysteresis loops of the SHG intensity measured under the excitation of the magnetic structure by (a) left circularly (LC) and(b) right circularly (RC) polarized fundamental radiation, DC magnetic field being parallel to the side of the Co triangles; (c) the DC magnetic field is parallel to the height of the triangles. P-polarized SH wave was detected.

shown in Fig. 4(c) is qualitatively similar to that measured for the linear pump polarization. In other words, we see that the macroscopic vortex magnetic moment results in the appearance of nonzero width of the SHG hysteresis loop at zero magnetic field. That allows us to distinguish different handedness of the vortex magnetization.

IV. PHENOMENOLOGICAL DESCRIPTION OF SHG IN VORTEX MAGNETIC STRUCTURES

In order to describe the experimental results on the SHG anisotropy from the structures under study we will consider the SHG response from triangular shaped nanodots. It is clear from the experiment that the SHG anisotropy and thus the SHG magnetic field dependencies are determined by the nonlinear optical response of an individual triangular particle. This may be attributed to the fact that the size of the dot is comparable to

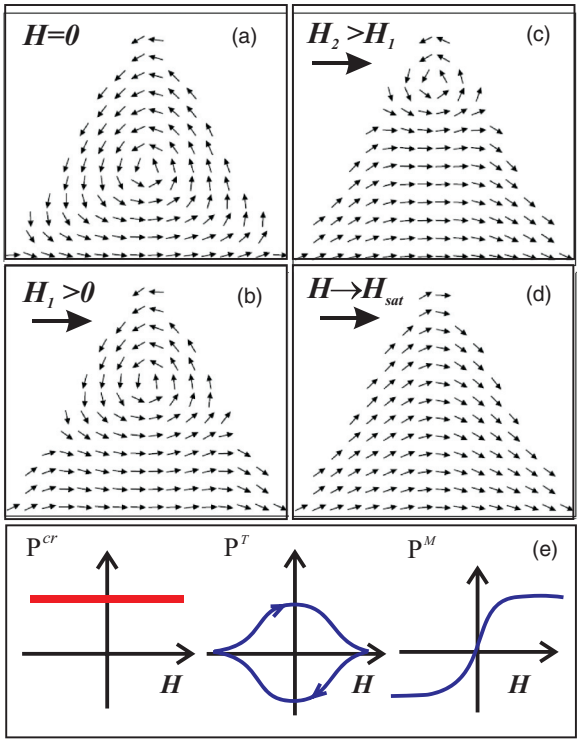

FIG. 5. (Color online) The result of micromagnetic simulations of spatial distribution of magnetic dipole moments in a single triangular-shaped nanodot for different values of the external magnetic field shown by an arrow (a)–(d). Schematic view of the magnetic field dependencies of $\mathbf{P}^{cr}$, $\mathbf{P}^{M}$, and $\mathbf{P}^{T}$ (e).

the wavelength of the fundamental radiation, while the lattice period is sufficiently larger.

Phenomenologically, the spatial distribution of magnetization may be defined by introducing the moments:

$$U^{(n)}_{ij\ldots m\eta} = \frac{1}{V}\int \underbrace{r_i r_j \ldots r_m}_{n-1} M_\eta dV, \qquad (1)$$

where V is the volume of a particle, r_l is the lth component of the radius vector, and M_η is the ηth component of the magnetization. The first rank tensor in Eq. (1) corresponds to the average magnetization $U^{(1)} \equiv \langle \mathbf{M} \rangle = \frac{1}{V}\int \mathbf{M} dV$ and equals to zero for vortex magnetic particles at $H = 0$. The results of micromagnetic simulations in a single triangular shaped magnetic dot for different values of the external magnetic field are shown in Figs. 5(a)–5(d). The simulations were performed using the ITL/NIST micromagnetics public code project.[25] A vortex magnetic structure is formed in the absence of magnetic field [Fig. 5(a)], the vortex core being placed in the geometrical center of a particle. Figure 5(c) shows the spatial distribution of $\mathbf{M}$ obtained for a magnetic field that is close to the saturation value $\mathrm{H_{sat}}$. It can be seen that the vortex structure is destroyed and averaged magnetization $\langle \mathbf{M} \rangle \neq 0$. Figure 5(b) shows an intermediate situation.

It is easy to show that the symmetric part of the second-rank tensor $U^{(2)s}_{i\eta} = \frac{1}{2}\{r_i M_\eta + M_i r_\eta\}$ is zero for the vortex magnetic particles, which are considered in our experiments. This stems from an antisymmetric distribution of $\mathbf{M}$ for a vortex magnetic state, $-M(r) = M(-r)$. On the contrary, the antisymmetric part $U^{(2)as}_{i\eta} = \frac{1}{2}\{r_i M_\eta - M_i r_\eta\} \neq 0$ in that case. It is known that an antisymmetric second-rank tensor is dual to a polar vector, which allows us to introduce a magnetic toroid moment $\mathbf{T} \propto \int [\mathbf{r} \times \mathbf{M}] dV$. This true vector can be used for the characterization of vortex magnetic distribution in magnetic dots.

Following the approach developed for a uniformly magnetized medium, the magnetization induced part of the SHG polarization can be described as $\mathbf{P}^M = \hat{\chi}^{(2)M}\mathbf{E}(\omega)\mathbf{E}(\omega)\mathbf{M}$.[26] Here and below for the sake of simplicity $\mathbf{M}$ denotes the averaged magnetization $\langle \mathbf{M} \rangle$. Analogously, the $\mathbf{T}$-induced contribution to the nonlinear polarization is $\mathbf{P}^T = \hat{\chi}^{(2)T}\mathbf{E}(\omega)\mathbf{E}(\omega)\mathbf{T}$. Here $\hat{\chi}^{(2)T}$ and $\hat{\chi}^{(2)M}$ are the corresponding parts of the second order susceptibility. Thus the SHG intensity from a single vortex magnetic dot can be described as a following function of the external magnetic field H:

$$I_{2\omega}(H) \propto |\mathbf{P}(M)|^2 = |\mathbf{P}^{cr} + \mathbf{P}^M(H) + \mathbf{P}^T(H)|^2, \qquad (2)$$

where $\mathbf{P}^{cr}$ is a nonmagnetic (crystallographic) component of the nonlinear polarization. The three terms in Eq. (2) are described by various dependencies on the magnetic field. The first one is constant, $\mathbf{P}^M(H)$ is antisymmetric in H and is zero for $H = 0$. The third contribution is symmetric with respect to $H = 0$ and has the opposite signs for the different branches of the hysteresis loops. Schematically, these dependencies are shown in Fig. 5(d).

It should be stressed that $\mathbf{P}^T$ and $\mathbf{P}^H$ reveal different dependencies on the external magnetic field. Indeed, $\mathbf{T}$ is a real vector that is oriented along the normal to the surface of vortex Co particles, it reaches its maxima at $H = 0$ and is zero for the saturating H values. The toroid moment changes its sign as the vorticity of magnetic particles is changed, so that $\mathbf{P}^T$ has the opposite orientations for different branches of the SHG hysteresis loops.

On the contrary, $\mathbf{P}^M$ is induced by an axial susceptibility tensor that introduces additional magnetic symmetry operations. In particular, reversal of magnetization leads to change of the sign of $\mathbf{P}^M$ and is responsible for the appearance of magneto-optical Kerr effects at the SHG wavelength that can be seen for the saturating magnetic fields (see Figs. 3 and 4).

To describe the SHG anisotropy and hysteresis loops, the symmetry of all the SHG susceptibility tensors $\hat{\chi}^{(2)cr}$, $\hat{\chi}^{(2)T}$ and $\hat{\chi}^{(2)M}$ should be analyzed for the case of a triangular-shaped Co nanodot. The crystallographic susceptibility $\hat{\chi}^{cr}$ tensor has the following components that contribute to the p-polarized SHG that is measured in the experiment:[16]

$$\begin{aligned} &\chi^{cr}_{yyz} = \chi^{cr}_{yzy}, \quad \chi^{cr}_{yyy} = -\chi^{cr}_{yxx} \\ &\chi^{cr}_{zxx} = \chi^{cr}_{zyy}, \chi^{cr}_{zzz}. \end{aligned} \qquad (3)$$

The symmetry of these components determine the $3m$ symmetry of an individual triangular nanodot, so that $\mathbf{P}^{cr} \propto |a + b \sin 3\psi|$ for both linear and circular polarization of the fundamental radiation,[16] where ψ is the azimuthal angle of rotation. The corresponding approximation is shown by solid lines in Fig. 2 and is in good agreement with the experiment.

As a nonzero magnetic field oriented along the side of a triangular-shaped Co particle, $M \parallel (OX)$ (see the coordinate frame in Fig. 1), the average homogeneous magnetization reduces the symmetry of the SHG response from $3m$ to a mirror

plane symmetry. Thus the following magnetization-induced SHG susceptibility components appear:[17]

$$\begin{aligned}\chi^M_{yxxX},\chi^M_{yyyX},\chi^M_{yzzX},\chi^M_{yyzX} &= \chi^M_{yzyX},\\ \chi^M_{zxxX},\chi^M_{zyyX},\chi^M_{zzzX},\chi^M_{zyzX} &= \chi^M_{zzyX},\end{aligned} \tag{4}$$

where the last subscript index denotes the orientation of **M**.

Finally, the following nonzero components induced by the **T** vector exist:

$$\begin{aligned}&\chi^T_{yyzZ} = \chi^T_{yzyZ}, \quad \chi^T_{yyyZ} = -\chi^T_{yxxZ}\\ &\chi^T_{zxxZ} = \chi^T_{zyyZ},\chi^T_{zzzZ};\end{aligned} \tag{5}$$

The $\hat{\chi}^{(2)}$ components expressed by Eqs. (3)–(5) determine the SHG magnetic field dependencies for a particular combination of polarizations of the fundamental and SHG radiation. In general, one can write for the ith Cartesian component of **P**:

$$P_i = \chi^{cr}_{ijk}E_jE_k + e^{i\phi_1}\chi^T_{ijkl}E_jE_kT_l + e^{i\phi_2}\chi^M_{ijkl}E_jE_kM_l, \tag{6}$$

where ϕ_1 and ϕ_2 are the relative phase shifts and the summation over the indices is supposed.

In the simplest case of a nonabsorbing nonlinear medium and linearly polarized SHG and fundamental radiation, the phase shifts ϕ_1 and ϕ_2 are 90°, so that there is no interference between $\mathbf{P}^M$, $\mathbf{P}^T$ and the crystallographic contribution to **P** in Eq. (2). Therefore there should be no linear in magnetization effect in the SHG intensity induced by **M** and **T**. On the contrary, for a circularly polarized incident light and the two orientations of the plane of incidence (mirror plane *YOZ* and perpendicular to the mirror plane *XOZ*) we get:

$$\mathbf{E}^{(YOZ)} = -\mathbf{e}_x \pm i(\mathbf{e}_y\sin\theta + \mathbf{e}_z\cos\theta), \tag{7}$$

$$\mathbf{E}^{(XOZ)} = \mathbf{e}_y \pm i\,(\mathbf{e}_x\sin\theta + \mathbf{e}_z\cos\theta)\,, \tag{8}$$

where θ is the angle of incidence and "±" stands for two circular polarizations of the fundamental wave. In this case the phase shift between Cartesian components of the electric field **E** leads to the interference between $\mathbf{P}^{cr}$ and $\mathbf{P}^M$. Thus linear in **M** and **T** effects in the SHG intensity and the corresponding SHG magnetic hysteresis loops can be observed for the circular polarization of the fundamental light.

It is worth noting that this effect exists in noncentrosymmetric dots and vanishes for laterally isotropic (circular) particles. Moreover, SHG hysteresis also vanishes in nonabsorbing dots if the plane of incidence of the fundamental beam coincides with the mirror plane of the particle due to the symmetry considerations described above, while this restriction is avoided if the magnetic medium is nontransparent.

Thus the symmetry analysis has shown that in the case of the circularly polarized fundamental beam, nonzero components of the susceptibility tensors $\hat{\chi}^T$ and $\hat{\chi}^M$ exist. The SHG magnetic hysteresis loops shown in Fig. 4 can be approximated by the expression (2). In our approximation model we assumed that $P^M(H) \sim M(H) = A_1 \cdot \arctan(H - H_c)$, where $M(H)$ is average magnetization and H_c is coercivity and $P^T(H) = A_2 \cdot e^{-\frac{H^2}{\sigma}}$. Solid lines in Figs. 4(a) and 4(b) are the result of the corresponding approximation of the experimental data, which are in reasonable agreement. It stems from the approximation (Fig. 4) that the phase shift ϕ_1 is 98°±5° and ϕ_2 is 102°±5°, which is close but still differ from the $\pi/2$ value for nonabsorbing media. The obtained amplitudes A_1 and A_2 equal 0.15 ± 0.02 and 0.09 ± 0.03 correspondingly (when the amplitude of nonmagnetic response is normed to 1).

Thus we may conclude that the appearance of the magnetic toroid moment is clearly seen in the SHG response for the circular polarization of the fundamental radiation and corresponds to a nonzero width of the SHG magnetic hysteresis loop at zero value of the external magnetic field. At the same time, such an effect for the linear polarization is much less pronounced.

V. CONCLUSION

Summing up, we have studied the SHG hysteresis loops in a regular array of Co triangular nanodots for different polarizations of the fundamental radiation. We demonstrate the appearance of two magnetization-induced effects, the first one being linear in the average magnetization and the second one induced by a macroscopic magnetic toroid moment. We show that for circularly polarized pump radiation the SHG hysteresis loop at $H = 0$ reveals a nonzero width, which undoubtedly indicates the appearance of the toroid moment in the formation of the SHG response. A phenomenological description of the SHG process in vortex magnetic structures is developed.

ACKNOWLEDGMENTS

The authors are thankful to A. A. Fraerman for fruitful discussions and to O. L. Ermolayeva for the micromagnetic simulations. This work was partially supported by RFBR Grant Nos. 13-02-01102 and 12-02-33039, by the Federal Program of the Russian Ministry of Education and Science (Grant Nos. 8393 and 8565), and by the "Dynasty" foundation.

[1]F. Hache, D. Ricard, and C. Flytzanis, J. Opt. Soc. Am. B **3**, 1647 (1986).

[2]O. A. Aktsipetrov, A. A. Fedyanin, E. D. Mishina, A. A. Nikulin, A. N. Rubtsov, C. W. van Hasselt, M. A. C. Devillers, and Th. Rasing, Phys. Rev. Lett. **78**, 46 (1997).

[3]V. G. Avramenko, T. V. Dolgova, A. A. Nikulin, A. A. Fedyanin, O. A. Aktsipetrov, A. F. Pudonin, A. G. Sutyrin, D. Y. Prohorov, and A. A. Lomov, Phys. Rev. B **73**, 155321 (2006).

[4]I. D. Mayergoyz, D. R. Fredkin, and Z. Zhang, Phys. Rev. B **72**, 155412 (2005).

[5]V. L. Brudny, B. S. Mendoza, and W. L. Mochan, Phys. Rev. B **62**, 11152 (2000).

[6]V. K. Valev, A. V. Silhanek, Y. Jeyaram, D. Denkova, B. De Clercq, V. Petkov, X. Zheng, V. Volskiy, W. Gillijns, G. A. E. Vandenbosch, O. A. Aktsipetrov, M. Ameloot, V. V. Moshchalkov, and T. Verbiest, Phys. Rev. Lett. **106**, 226803 (2011).

[7]Evgeni Y. Poliakov, Vadim A. Markel, Vladimir M. Shalaev, and Robert Botet, Phys. Rev. B **57**, 14901 (1998).

[8]O. A. Aktsipetrov, E. M. Kim, R. V. Kapra, T. V. Murzina, A. F. Kravets, M. Inoue, S. V. Kuznetsova, M. V. Ivanchenko, and V. G. Lifshits, Phys. Rev. B **73**, 140404 (2006).

[9] A. Fert, Rev. Mod. Phys. **80**, 1517 (2008).
[10] C. L. Chien, F. Q. Zhu, and J.-G. Zhu, Phys. Today **60**(6), 40 (2007).
[11] Bas B. Van Aken, Jean-Pierre Rivera, Hans Schmid, and Manfred Fiebig, Nature (London) **449**, 702 (2007).
[12] S. Prosandeev, I. Ponomareva, I. Kornev, and L. Bellaiche, Phys. Rev. Lett. **100**, 047201 (2008).
[13] Mi-Young Im, P. Fischer, K. Yamada, T. Sato, Sh. Kasai, Y. Nakatani, and T. Ono, Nat. Commun. **3**, 983 (2012).
[14] O. G. Udalov, M. V. Sapozhnikov, E. A. Karashtin, B. A. Gribkov, S. A. Gusev, E. V. Skorohodov, V. V. Rogov, A. Yu. Klimov, and A. A. Fraerman, Phys. Rev. B **86**, 094416 (2012).
[15] S. Yakata, M. Miyata, S. Nonoguchi, H. Wada, and T. Kimura, Appl. Phys. Lett. **97**, 222503 (2010).
[16] P. Guyot-Sionnest, W. Chen, and Y. R. Shen, Phys. Rev. B **33**, 8254 (1986).
[17] R.-P. Pan, H. D. Wei, and Y. R. Shen, Phys. Rev. B **39**, 1229 (1989).
[18] Y. Z. Wu, R. Vollmer, H. Regensburger, X. F. Jin, and J. Kirschner, Phys. Rev. B **63**, 054401 (2000).
[19] H. A. Wierenga, M. W. J. Prins, D. L. Abraham, and Th. Rasing, Phys. Rev. B **50**, 1282 (1994).
[20] V. L. Krutyanskiy, I. A. Kolmychek, E. A. Ganshina, T. V. Murzina, P. Evans, R. Pollard, A. A. Stashkevich, G. A. Wurtz, and A. V. Zayats, Phys. Rev. B **87**, 035116 (2013).
[21] N. A. Spaldin, M. Fiebig, and M. Mostovoy, J. Phys.: Condens. Matter **20**, 434203 (2008).
[22] M. Fiebig, V. V. Pavlov, and R. V. Pisarev, J. Opt. Soc. Am. B **22**, 96 (2005).
[23] A. A. Fraerman, S. A. Gusev, L. A. Mazo, I. M. Nefedov, Y. N. Nozdrin, I. R. Karetnikova, M. V. Sapozhnikov, I. A. Shereshevskii, and L. V. Sukhodoev, Phys. Rev. B **65**, 064424 (2002).
[24] A. V. Melnikov, A. A. Nikulin, and O. A. Aktsipetrov, Phys. Rev. B **67**, 134104 (2003).
[25] M. Fiebig, V. V. Pavlov, and R. V. Pisarev, OOMMF User's Guide, Interagency Report NISTIR 6376, National Institute of Standards and Technology, Gaithersburg, http://math.nist.gov/oommf.
[26] V. N. Gridnev, V. V. Pavlov, R. V. Pisarev, A. Kirilyuk, and Th. Rasing, Phys. Rev. B **63**, 184407 (2001).